SUPPLEMENTARY INFORMATION

Electronic Localization in $CaVO_3$ Films via Bandwidth Control

D.E. McNally,[1] Xingye Lu,[1] J. Pelliciari,[1,*] S. Beck,[2] M. Dantz,[1] M. Naamneh,[1] T. Shang,[1,3] M. Medarde,[4] C.W. Schneider,[5] V.N. Strocov,[1] E.V. Pomjakushina,[6] C. Ederer,[2] M. Radovic,[1,†] and T. Schmitt[1,‡]

[1] *Photon Science Division, Paul Scherrer Institut, CH-5232, Villigen, Switzerland*
[2] *Materials Theory, ETH Zurich, Wolfgang-Pauli-Strasse 27, CH-8093 Zurich, Switzerland*
[3] *Institute of Condensed Matter Physics, Ecole Polytechnique Federale de Lausanne (EPFL), CH-1015 Lausanne, Switzerland*
[4] *Laboratory for Scientific Developments and Novel Materials, Paul Scherrer Institut, CH-5232 Villigen PSI, Switzerland*
[5] *Laboratory for Multiscale Materials Experiments, Paul Scherrer Institut, CH-5232 Villigen PSI, Switzerland*
[6] *Photon Science Division, Paul Scherrer Institut, CH-5232 Villigen PSI, Switzerland*

(Dated: December 10, 2018)

DETAILS OF THE EXPERIMENTAL METHODS

X-ray Absorption Spectroscopy (XAS) and Resonant Inelastic X-ray Scattering (RIXS) experiments were carried out at the ADRESS beamline of the Swiss Light Source at the Paul Scherrer Institute [1]. All measurements were performed at grazing incidence with the x-rays incident at 15° with respect to the sample surface and with σ or π polarization. The scattering angle was fixed at 130°. We set the spectrometer [2] in the high throughput configuration, using the 1500 lines per mm variable line spacing (VLS) spherical grating [3] as well as the newly installed CCD camera that provides sub-pixel spatial resolution [4]. The beamline exit slit was 20 μm. This setup yielded a total energy resolution (full width at half max FWHM) of around 60 meV.

Thin films of $CaVO_3$ and $SrVO_3$ were grown on $SrTiO_3$ (100) and $NdGaO_3$ (110) substrates respectively by pulsed laser deposition (PLD). Films were deposited in high vacuum 10^{-7} mbar (base pressure: 10^{-9} mbar) with substrate temperature of 680 ° C. Films were cooled at a rate of 20 ° C per minute. In-situ reflection high-energy electron diffraction (RHEED) was used to monitor film growth, thickness, and homogeneity.

RHEED patterns of CVO films with different thicknesses recorded at the growth temperature and at the room temperature (RT) after deposition revealed a small structural dissimilarity. The RHEED patterns in Figure 1 of films with thicknesses of above 6 are nearly identical but less spotty and more streaky than the 6u.c. thick film. This indicates the occurrence of small domains in CVO film with thickness above 6 u.c. (Fig. 1).

We find that the optimal growth condition is in high vacuum at 10^{-7} mbar presure (base pressure: 10^{-9} mbar). In-situ and ex-situ annealing in oxygen has been tested and we find that the film surface quality rapidly changed upon the introduction of only 10^{-4} mbar Oxygen at 600 ° C (see RHEED pattern in Fig. 2). With further increasing of Oxygen pressure (0.1 mbar), the film quality degraded significantly. Therefore, for the thinner films (15 u.c., 10 u.c., 6 u.c., 4 u.c. $CaVO_3$) a thin 2 nm $SrTiO_3$ overlayer was deposited to protect against environmental degradation upon removal from PLD chamber. Time outside vacuum was minimized to few hours and no degradation was observed over a timescale of weeks.

RHEED patterns of capped CVO films recorded at room temperature (RT) after deposition revealed a structural dissimilarity (Fig 3), possibly caused by octahedral rotation. The RHEED pattern of the capped 6 u.c CVO thick layer shows very clear indications for lowering of the surface symmetry (reconstruction streaks are indicated by arrows in Fig. 3). The fact that the uncapped film with the same thicknesses does not show structural reconstruction effects in form of additional RHEED streaks leads us to conclude that the structural reconstruction observed in the capped films is induced or stabilized by the STO capping layer.

Ex-situ x-ray diffraction (XRD) θ-2θ scans were performed on a Seifert four-circle x-ray diffractometer and confirmed the formation of crystalline $CaVO_3$ films with no indication of secondary phases as shown in Figure 4. Reciprocal space mapping of the 50 u.c. $CaVO_3$ film revealed the thicker films were relaxed from the substrate (Figure 3). These data display our films are of the same quality as those previously reported [5, 6].

Four-probe resistance measurements were carried out on a Quantum Design Physical Property Measurement System (PPMS) using a homemade mask with metallic point contacts. A zoom in on the resistance data for the CVO films is shown in Figure 6.

FITTING AND ANALYSIS OF RIXS DATA

Figure 7 presents fits to the electron-hole pair excitations that were presented in Figure 3a of the main text. The results of these fits (position and bandwidth of the asymmetric Lorentzian) are presented in the bottom panel of Figure 3d of the main text.

Figure 8 presents the derivative of the band excitations presented in Figure 3c of the main text. The bandwidth is indicated by the double arrows chosen by the turning points of the first derivative.

It is important to rule out other possible excitations that could account for the Raman mode R1. As bulk $CaVO_3$ is not magnetically ordered we can rule out sharp magnetic excitations at this energy scale. Phonons are reported in $CaVO_3$ below 50 meV [7] although we are not aware of any published Raman scattering in the region 50 meV - 500 meV. We note that crystal field "dd" excitations were reported in the isostructural insulating $3d^1$ compounds $LaTiO_3$ and $YTiO_3$ at ≈ 0.25 eV [8]. However, there are several reasons we can rule out dd excitations as the sole root of the low energy Raman peak in $CaVO_3$ in Figure 3a of the main text. First, the orthorhombic distortion that lifts the degeneracy of t_{2g} orbitals is significantly larger in $YTiO_3$ while the measured peak for our 50 u.c. $CaVO_3$ film is at a higher energy scale. Second, we also observe this peak in $SrVO_3$, that is a $3d^1$ compound with cubic symmetry. Thus, there is no splitting of the t_{2g} manifold and we should not see any intra-t_{2g} excitations [9]. However, our $SrVO_3$ spectrum displays a strong peak with a maximum at ≈ 0.5 eV, a higher energy scale than the peak in

sample	Temperature (RHHED)	6 u.c.	12 u.c.	24 u.c.	48 u.c.
I	680 C	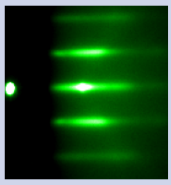	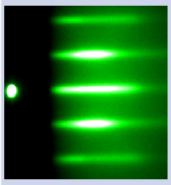	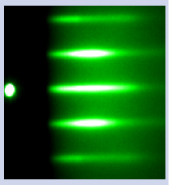	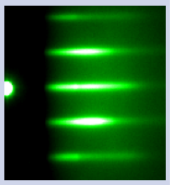
	Room T	X	X	X	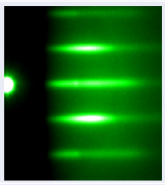
II	680 C	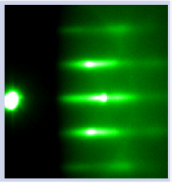	X	X	X
	Room T	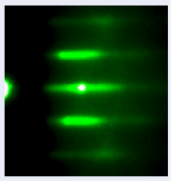	X	X	X

FIG. 1. RHEED patterns of uncapped CVO films with different thickness. The RHEED pattern of 6 u.c. CVO film is spotty while CVO film thicker than 6 u.c. show streaky patterns.

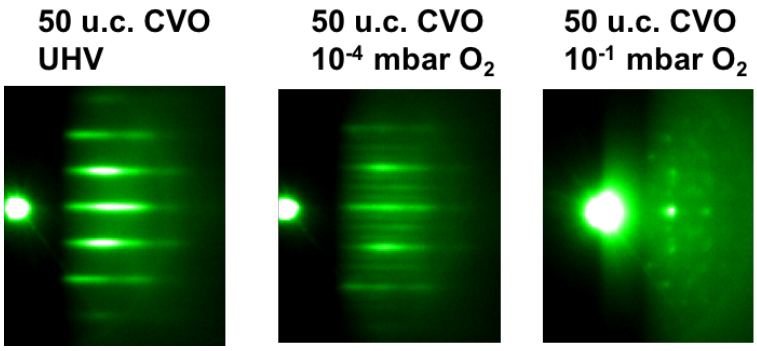

FIG. 2. RHEED pattern of CVO film after the growth and after introducing Oxygen.

$CaVO_3$. As we traverse the thickness-induced MIT we might expect dd excitations to become more prominent in the spectra as a result of the increased orthorhombicity due to the tensile strain induced by lattice mismatch with $SrTiO_3$ substrate [10]. However, the energy scale of these dd excitations remains small $\approx$ 100 meV for moderate orthorhombic distortions of $3d^1$ systems and a confident fitting including a dd peak near this energy scale and an electron-hole peak at higher energy was not possible.

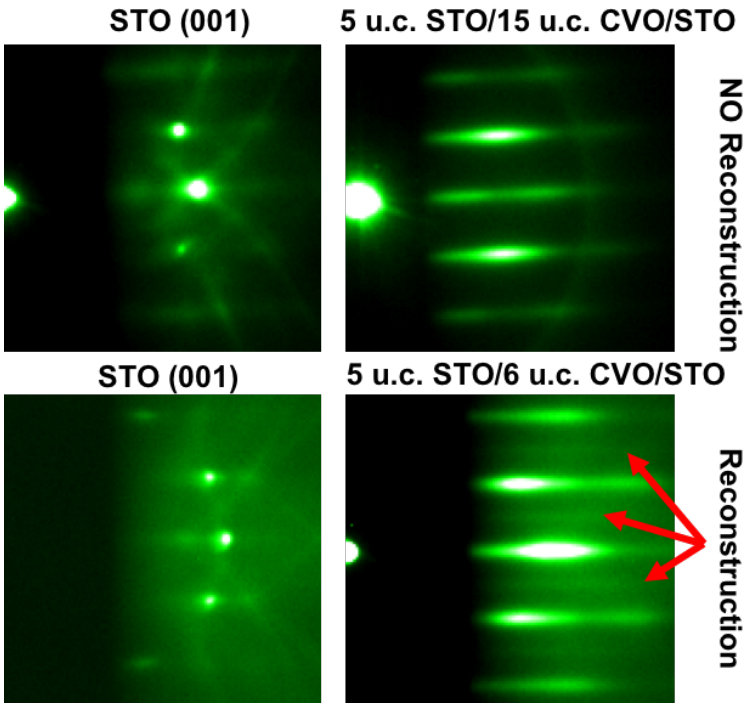

FIG. 3. RHEED pattern of STO substrates and capped CVO films. The RHEED pattern of the 6 u.c thick CVO film capped with 5 u.c. STO shows clear indication of different crystal ordering with lower symmetry than the capped 15 u.c CVO film.

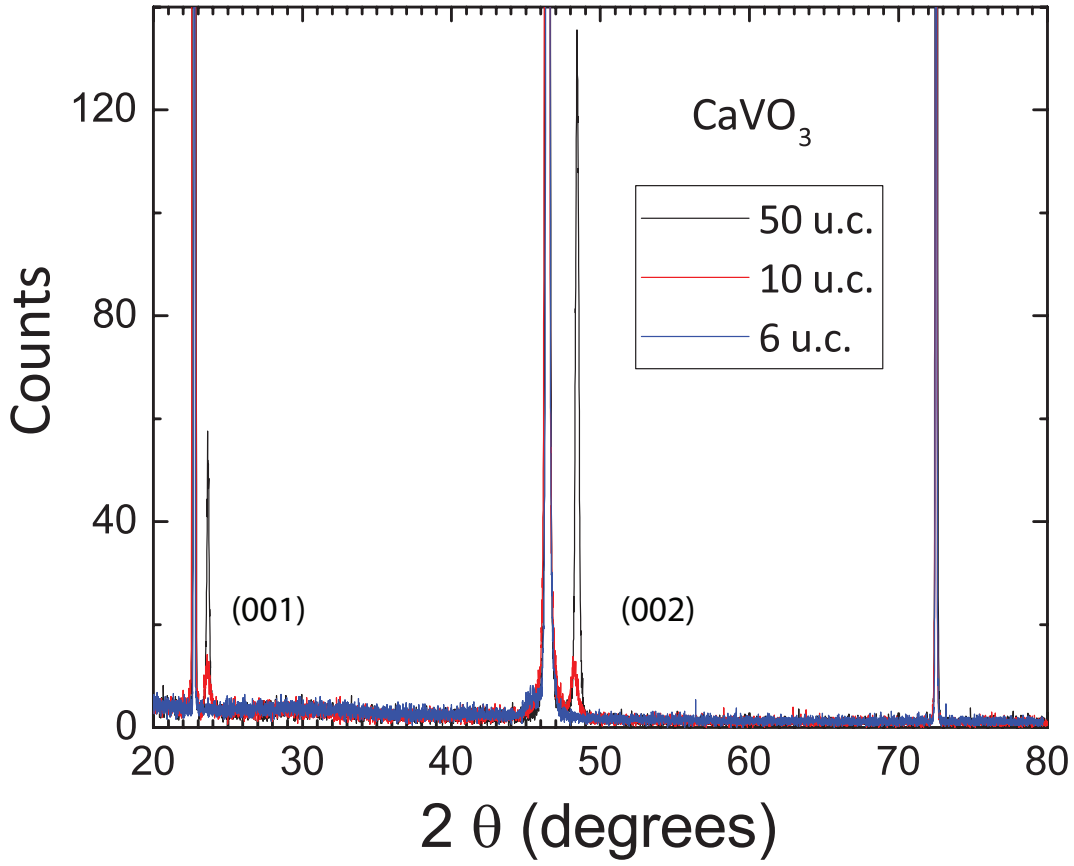

FIG. 4. X-ray diffraction θ-2θ scans of films indicated. Film reflections are indicated in the pseudo-cubic notation.

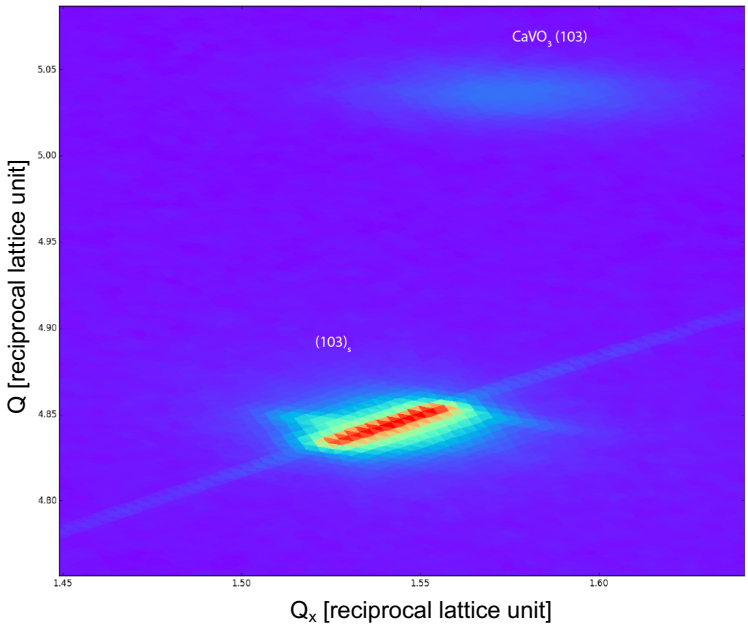

FIG. 5. Reciprocal space mapping around the (103) substrate and film peaks indicated for a 50 u.c. $CaVO_3$ film.

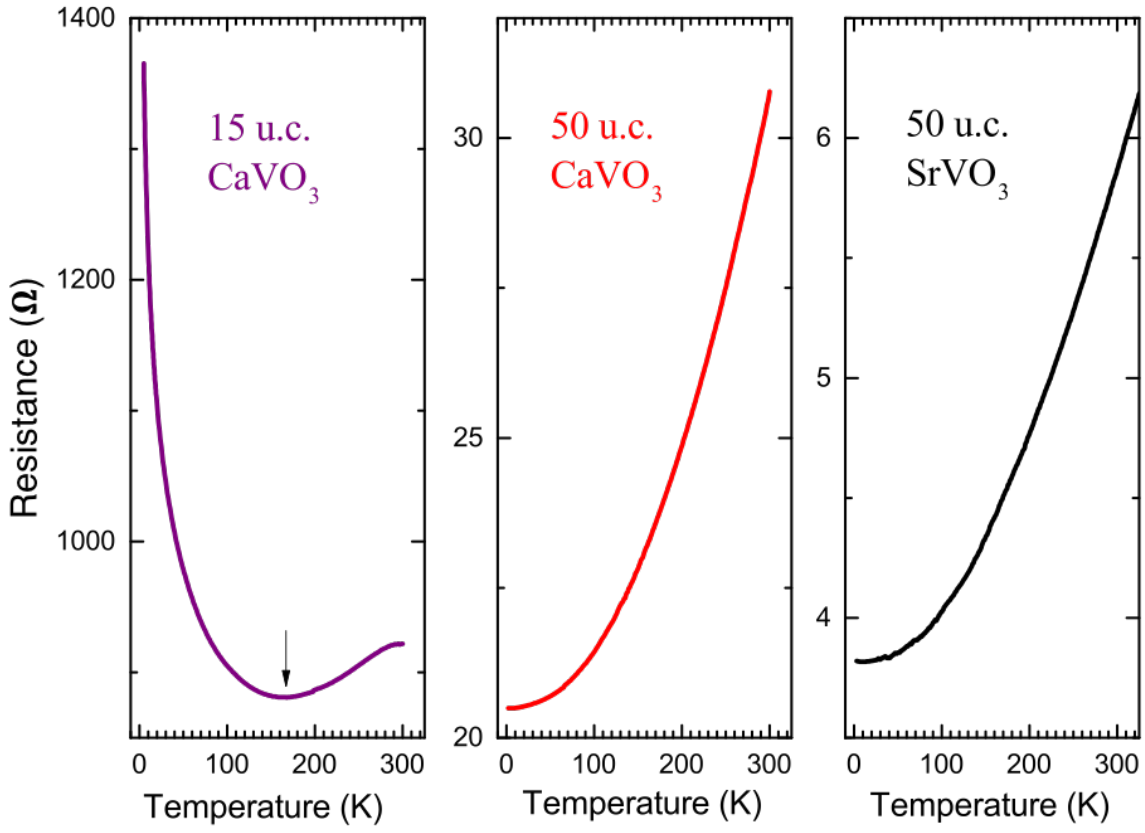

FIG. 6. Zoom in on the Resistance curves presented in Figure 1 of the main text for the films indicated. The arrow indicates where the upturn occurs for the 15 u.c. film.

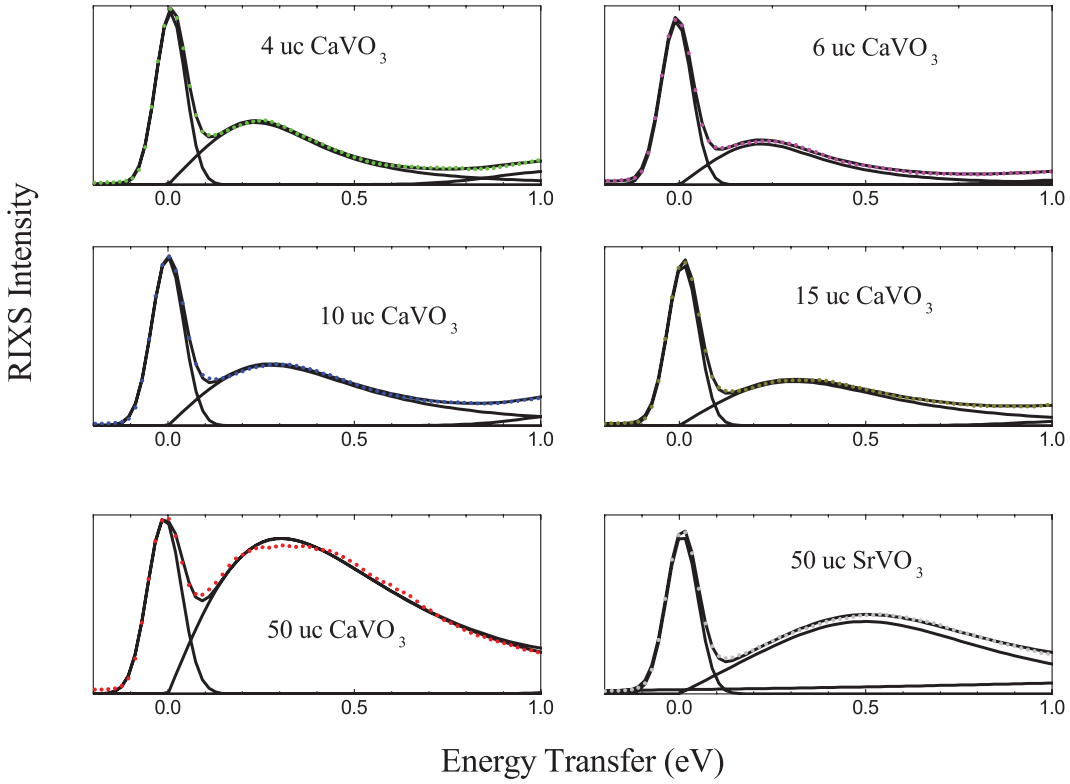

FIG. 7. Fits to the electron hole excitations presented in Figure 3a of the main text. We have fit to the sum of a Gaussian for the elastic line, an asymmetric Lorentzian for the electron-hole contribution and an additional Gaussian for the tail of the high energy crystal field excitations.

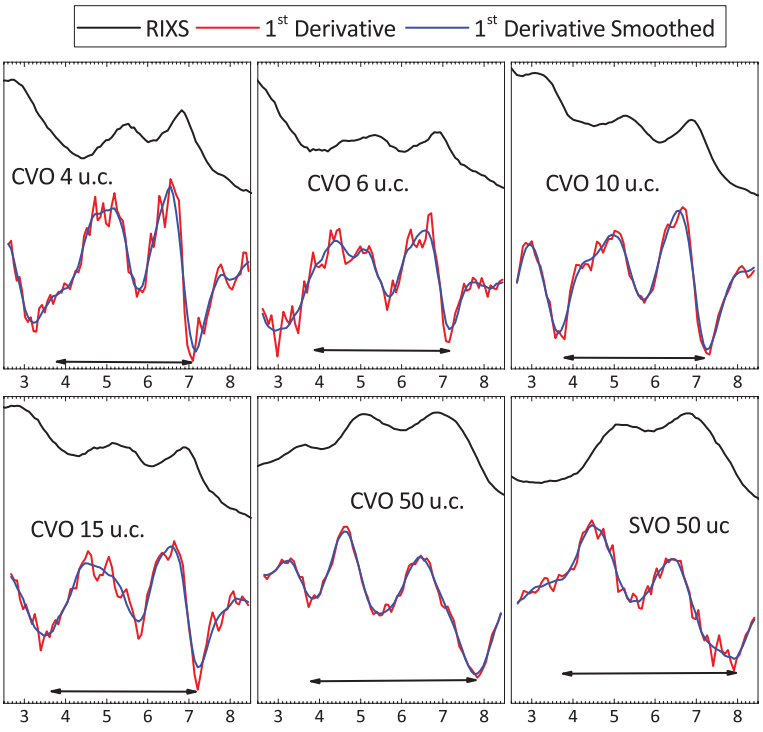

FIG. 8. Derivative of the RIXS spectra presented in Figure 3c of the main text. The double arrow indicates the bandwidth that is plotted in Figure 3d (top panel) of the main text.

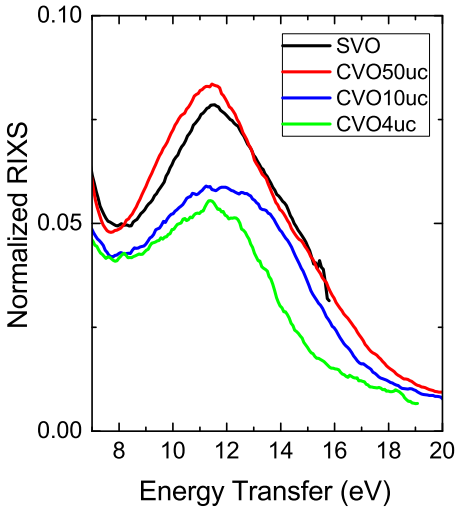

FIG. 9. RIXS normalized to the integrated intensity showing the V-O band's hybridization change for the compounds indicated.

REFERENCES

* Current address: Department of Physics, Massachusetts Institute of Technology, Cambridge, Massachusetts 02139, USA
† milan.radovic@psi.ch
‡ thorsten.schmitt@psi.ch

[1] V.N. Strocov, T. Schmitt, U. Flechsig, T. Schmidt, A. Imhof, Q. Chen, J. Raabe, R. Betemps, D. Zimoch, J. Krempasky, X. Wang, M. Grioni, A. Piazzalunga, and L. Patthey, *High-resolution soft X-ray beamline ADRESS at the Swiss Light Source for resonant inelastic X-ray scattering and angle-resolved photoelectron spectroscopies*, J. Synchrotron Rad. **17**, 631–643 (2010).

[2] G. Ghiringhelli, A. Piazzalunga, C. Dallera, G. Trezzi, L. Braicovich, T. Schmitt, V.N. Strocov, R. Betemps, L. Patthey, X. Wang, and M. Grioni, *SAXES, a high resolution spectrometer for resonant x-ray emission in the 400-1600 eV energy range*, Rev. Sci. Instr. **77**, 113108 (2006).

[3] T. Schmitt, V.N. Strocov, K.-J. Zhou, J. Schlappa, C. Monney, U. Flechsig, and L. Patthey, *High-resolution resonant inelastic X-ray scattering with soft X-rays at the ADRESS beamline of the Swiss Light Source: Instrumental developments and scientific highlights*, J. Elec. Spec. & Rel. Phen. **188**, 38-46 (2013).

[4] M. R. Soman, D. J. Hall, J. H. Tutt, N. J. Murray, A. D. Holland, T. Schmitt, J. Raabe, and B. Schmitt, *Developing a CCD camera with high spatial resolution for RIXS in the soft X-ray range*, Nucl. Instrum. Methods Phys. Res. A 731, 47 (2013).

[5] M. Liberati, R.V. Chopdekar, V. Mehta, E. Arenholz, and Y. Suzuki, *Epitaxial growth and characterization of $CaVO_3$ thin films*, Journal of Magnetism and Magnetic Materials, **321**, 2852–2854 (2009).

[6] S. Backes, T.C. Rodel, F. Fortuna, E. Frantzeskakis, P. Le Fevre, F. Bertran, M. Kobayashi, R. Yukawa, T. Mitsuhasi, M. Kitamura, K. Horiba, H. Kumigashira, R. Saint-Martin, A. Fouchet, B. Berini, Y. Dumont, A.J. Kim, F. Lechermann, H.O. Jeschke, M.J. Rozenberg, R. Valenti, and A.F. Santander-Syro, *Hubbard band versus oxygen vacancy states in the correlated electron metal $SrVO_3$*, Phys. Rev. B, **94** 241110(R) (2016).

[7] H. Makino, I. H. Inoue, M. J. Rozenberg, I. Hase, Y. Aiura, and S. Onari, *Bandwidth control in a perovskite-type $3d^1$-correlated metal $Ca_1xSr-xVO_3$.II. Optical spectroscopy*, Phys. Rev. B **58**, 4384 (1998).

[8] C. Ulrich, L.J.P. Ament, G. Ghiringhelli, L. Braicovich, M. Moretti Sala, N. Pezzotta, T. Schmitt, G. Khaliullin, J. van den Brink, H. Roth, T. Lorenz, and B. Keimer, *Momentum Dependence of Orbital Excitations in Mott-Insulating Titanates*, Phys. Rev. Lett., **103**, 107205 (2009).

[9] E. Pavarini, A. Yamasaki, J. Nuss, and O.K. Andersen, *How chemistry controls electron localization in $3d^1$ perovskites: a Wannier function study*, N. J. Phys., **7**, 188 (2005).

[10] Sophie Beck, Gabriele Sclauzero, Uday Chopra, and Claude Ederer *Metal-insulator transition in $CaVO_3$ thin films: Interplay between epitaxial strain, dimensional confinement, and surface effects*, Phys. Rev. B **97**, 075107 (2018).